

RESEARCH ARTICLE

Transport Phenomena and Fluid Mechanics

Settling and fluidization of tall cylinders in solid-liquid suspensions

Jos J. Derksen School of Engineering, University of Aberdeen,
Aberdeen, UK

Correspondence

Jos J. Derksen, School of Engineering,
University of Aberdeen, Aberdeen, UK.
Email: jderksen@abdn.ac.uk**Abstract**

We numerically study how rigid solid cylinders with a length over diameter aspect ratio of 10 settle through suspensions consisting of uniformly sized solid spheres and Newtonian liquid. We identify regimes with preference for horizontal settling and vertical settling of the cylinders dependent on the overall solids volume fraction (in the range of 0–0.58) and the Archimedes number of the cylinders. These insights we use to interpret the behavior of fluidized suspensions consisting of mixtures of spheres and cylinders with an emphasis on cylinder orientation distributions and slip velocities between solids and liquid phase. The three-dimensional and time-dependent simulations explicitly resolve the solid-liquid interfaces by applying an immersed boundary method contained in a lattice-Boltzmann flow solver.

KEYWORDS

lattice-Boltzmann method, liquid fluidization, non-spherical particles, particle-resolved simulation

1 | INTRODUCTION

Sedimentation and solid-liquid fluidization are widely studied topics given their relevance in natural and engineered processes. Settling and fluidization velocities and their relation to particle and fluid properties and solids loading impact process time and process performance. Relative velocity (slip) between liquid and solids determine heat and mass transfer over (solid-liquid) interfaces. Not only average velocities but also velocity fluctuations are important in this respect, with the fluctuations induced by the randomness of particle assemblies and possibly turbulence. Numerical simulations of flow phenomena at length scales comparable to particle size are a way to probe how the microstructure of suspensions and associated momentum and mass transfer mechanisms depend on process conditions and (solid and liquid) material properties. Such computational activities applied to suspensions containing spherical particles have led to important insights on drag forces and

particle-related (collisional and streaming) stress.^{1–4} Given various types of applications, but also given the additional (orientational) degrees of freedom that give rise to interesting flow phenomena, investigating non-spherical and non-uniform collections of particles is relevant.

When it comes to applications, one process we have in mind is biomass conversion. Conversion of biomass (gasification, pyrolysis) frequently uses fluidized bed reactors to achieve homogeneous conditions for high levels of heat transfer and intensive mixing.⁵ Fluidizability of biomass, which in general is a heterogeneous, fibrous material, is enhanced by mixing with sand.^{6,7} Another application that has our interest is processing of materials for lithium-ion battery electrodes^{8,9} that involves dispersing (among more) cylinder-shaped particles at very high volume fractions in a continuous carrier liquid. From the perspective of such applications it is worthwhile to study the interactions between fibers, spherical particles, and the continuous phase fluid they are

This is an open access article under the terms of the [Creative Commons Attribution-NonCommercial-NoDerivs](https://creativecommons.org/licenses/by-nc-nd/4.0/) License, which permits use and distribution in any medium, provided the original work is properly cited, the use is non-commercial and no modifications or adaptations are made.

© 2023 The Author. *AIChE Journal* published by Wiley Periodicals LLC on behalf of American Institute of Chemical Engineers.

immersed in under fluidized conditions. In this article, we do this by means of numerical simulations.

The aim is to achieve insight in the behavior of the cylinders, their orientation relative to the direction of gravity, and their relative velocity with respect to the spheres and the fluid. In our previous article on the topic of co-fluidization of cylinders and spheres,¹⁰ the focus was on the effect of the length over diameter aspect ratio of the cylinders (varied between 4 and 10) and the relative amount of cylinder volume at a fixed overall solids volume fraction of 0.4. It was shown that the cylinders “stir” the system; the more cylinders, the stronger the velocity fluctuations. In the present article, we study the effect of solids volume fraction on the orientation of tall (length over diameter ratio 10) cylinders. It shows, quite remarkably, the tendency of individual cylinders to orient horizontally in lean spheres suspensions (as the cylinders would also do in a single-phase system), and vertically in dense spheres suspensions with ramifications for co-fluidization of cylinders and spheres.

First, in this article, we consider a single cylinder in a bed of spheres and fluid with the cylinder settling through the spheres suspension and study its orientation and settling speed as a function of the solids volume fraction. Second, we progressively add more cylinders so as to also probe the mutual interaction between cylinders while being co-fluidized with the spheres.

The three-dimensional and time-dependent simulations explicitly account for particle shape. We use the lattice-Boltzmann method¹¹ to solve for the fluid flow on a lattice with a spacing much finer than the sizes of the particles and couple this to an immersed boundary method¹² to explicitly impose no-slip at the particle surfaces. This makes the simulations computationally expensive on a per-particle basis. We thus are only able to consider small-scale, mesoscopic systems containing of the order of 10^4 particles and use tri-periodic boundary conditions to make the systems representative samples contained in a much larger fluidized bed.

This article has been organized as follows. First the flow conditions are defined in terms of dimensionless numbers. The numerical procedures section that follows gives an overview of the methodology used for the simulations that we have in place, with references to previous articles that contain the details of the methodology. Then the physical parameter space that has been covered is described, and so are the numerical settings such as the resolution of the simulations in space and time. Section 5 consists of two parts: first the part on a single cylinder settling through a bed of fluidized spheres, second the part on co-fluidization of cylinders and spheres. A summary of the main findings and a research outlook conclude the article.

2 | FLOW SYSTEMS

The flow domains are three-dimensional with periodic boundary conditions in all three coordinate directions. Their size is denoted as $n_x \times n_y \times n_z$ in x , y , and z -direction respectively. Gravity acts in the negative z -direction: $\mathbf{g} = -g\mathbf{e}_z$ with \mathbf{e}_z the unit vector in z -direction. The domain contains Newtonian fluid with density ρ and kinematic viscosity ν . It

also contains one or more solid, rigid cylinders with length ℓ , diameter d , and density ρ_p , and it contains solid spheres all having the same diameter d and density ρ_p . Note that throughout this article the diameter of the spheres is the same as the diameter of the cylinder(s) and that spheres and cylinders have the same density. The overall solids volume fraction is denoted as $\langle\phi\rangle$, the cylinders volume fraction is $\langle\phi_c\rangle$, and their ratio $\langle\phi_c\rangle/\langle\phi\rangle$, which is the volume contained in cylinders over the total solids volume, is an input parameter that has been varied. The Archimedes number is defined as $Ar = (\gamma - 1)gd^3/\nu^2$ with $\gamma = \rho_p/\rho$.

With a fully periodic simulation domain we must make sure the overall system is force-balanced. To do so, and with the particles feeling net gravity in the negative z -direction, we apply a body force on the fluid in the positive z -direction: $\mathbf{f} = \langle\phi\rangle(\gamma - 1)\rho g\mathbf{e}_z$.⁴ In fluidization terms, this body force is the vertical pressure gradient that drives the fluidization process.

3 | NUMERICAL PROCEDURES

We use a variant of the lattice-Boltzmann (LB) method to solve for the fluid flow.^{13,14} The lattice is uniform and cubic with spacing Δ . The flow solutions evolve in time with a time step Δt . An immersed boundary method (IBM) has been used to represent the presence of the solid particles in the fluid.¹⁵ In this method, solid particle surfaces are covered by closely spaced sets of marker points with nearest neighbor spacing of 0.5Δ to 0.7Δ . At the marker points, no-slip is imposed by locally applying forces on the fluid such that the fluid velocity matches the solid surface velocity. The distribution of forces over the surface of each particle is integrated so as to determine the total hydrodynamic force and torque on that particle.

In addition to hydrodynamic forces, the particles feel close-range interaction forces. Identifying contact between non-spherical particles is more elaborate than for spheres. See, for example, the analytical approach for contact between cylinders as proposed by Kodam et al.¹⁶ In this article, a numerical approach has been followed where we identify close proximity of two particles using the same marker points as the ones of the IBM.¹⁷ There are two stages in close-range interaction. In the first stage, when the spacing between two marker points on two different particles falls below Δ , a lubrication force is activated.¹⁸ This is because at that stage the lattice cannot resolve the flow in the narrow space between the two particles anymore. The lubrication force has a radial and a tangential component, each of which is proportional to relative velocity between the particles in radial and tangential direction at the contact location. The radial proportionality constant for the lubrication force has been derived from the analytical expression for creeping flow between equally sized spheres with diameter d ¹⁹ but is also used for sphere-cylinder (SC) and cylinder-cylinder (CC) contacts given the lack of analytical expressions or other types of correlations for lubrication at such contacts. A reason for this choice is that the overwhelming majority of contacts in the simulations is sphere-sphere. Tangential lubrication is much weaker than radial lubrication¹⁹ which is accounted for by

making their proportionality constant one order of magnitude smaller than the radial one.¹⁷ Further details on contact identification and modeling are given in Ref. [17].

We have checked sensitivity to lubrication in a single-cylinder simulation by increasing the proportionality for SC contacts by a factor of two (we increase because cylinder surfaces are less curved than sphere surfaces). This change of lubrication parameters has no discernible effect on the statistics (averages and fluctuation levels) of cylinder's behavior as quantified by its settling velocity and orientation angle.

The second stage of close-range interaction kicks in at a closer proximity of $\Delta/3$. Then a linear radial spring force between the particles is activated which prevents them from overlapping. Note that we do not apply a tangential spring force, that is, we do not consider “dry” friction between the particles. As for the lubrication force, details, and parameter settings of the spring force are in Ref. [17].

After summing the close-range interaction forces for each particle, and determining the resulting torques per particle they are included in their linear and rotational equations of motion respectively. These we solve explicitly with a split-derivative method²⁰ with a time step equal to the LB time step Δt . For convenience, the rotational (Euler) equations of motion are solved in a reference frame attached to each particle. This approach requires back-and-forth mapping from the inertial xyz coordinate system to the local coordinate systems of the particles. For this, each particle is equipped with a quaternion that keeps track of its orientation which then facilitates the mapping operations.²¹

4 | SET-UP OF SIMULATIONS

Two classes of simulations have been performed. In the first class, a single cylinder with aspect ratio $\ell/d = 10$ and density ratio $\rho_p/\rho = 2.0$ settles through a suspension of spheres having a diameter equal to the cylinder diameter and the same density as the cylinder. For these simulations the overall solids volume fraction ranges from $\langle\phi\rangle \approx 0$ (actually $\langle\phi\rangle = 0.002$ with one cylinder and no spheres) to 0.58. Three values of the Archimedes number have been investigated: $Ar = 207, 864,$ and 1730 , with the middle value the base-case and most studied one. The Archimedes number was changed by changing the gravitational acceleration and/or the kinematic viscosity of the liquid.

The dimensions of the domain are $n_x \times n_y \times n_z = 15d \times 6d \times 45d$. As described above, fully periodic boundary conditions apply with forces explicitly balanced over the entire flow system. We need a tall domain (i.e., a large domain size in vertical [is z] direction) so as to correctly capture the wake that—at least for the low solids volume fraction cases—develops behind the cylinder.²² The relatively narrow dimension in the y-direction, along with the periodic boundary conditions, makes that, if the cylinder changes its orientation, it will preferentially do so by rotating along the y-axis. By comparing simulations that have $n_y = 6d$ with ones that have $n_y = 12d$ it was observed that the y-width of the flow domain hardly had a measurable impact on

the cylinder settling process after a dynamic steady state had been reached.

Initially spheres are placed randomly in the domain in a non-overlapping fashion. The cylinder is then placed in the center of the domain either vertically (along the z-axis) or horizontally (along the x-axis) and the spheres that would overlap with the cylinder's volume are removed. The simulation is started from zero solids and liquid velocity. The spatial resolution of the simulations is such that $d = 16\Delta$. Temporal resolution changes with the Archimedes number. For the base-case, that has $Ar = 864$, one viscous time scale $d^2/\nu = 6400\Delta t$. The simulations in this class will be referred to as single-cylinder settling simulations.

In the second class of simulations (referred to as co-fluidization simulations), multiple cylinders are co-fluidized with spheres. In terms of the setup of the simulations (including numerical settings), the only differences with the first class are the number of cylinders, which now is larger than one, and the domain size. The main aim of these simulations is to investigate to what extent the cylinders interact with one another as a function of the amount of cylinder volume relative to the total solids volume. The domain size has been fixed to $n_x \times n_y \times n_z = 15d \times 15d \times 30d$. Overall solids volume fractions are in the range $\langle\phi\rangle = 0.30 - 0.48$, and all simulations in this class have $Ar = 864$.

As compared with the single-cylinder settling simulations we do not need such tall domains since no lengthy wakes are able to develop behind the cylinders given the $\langle\phi\rangle$ levels considered. In a previous study,¹⁰ domain size effects have been assessed at comparable $\langle\phi\rangle$ and Ar values. Domains of $15d \times 15d \times 30d$ and $12d \times 12d \times 24d$ showed almost identical average and fluctuating velocities of co-fluidized cylinders with $\ell/d = 10$. Next to the overall solids volume fraction, the amount of solid volume contained in the cylinders relative to the total solids volume has been varied in the range $\langle\phi_c\rangle/\langle\phi\rangle = 0.05$ to 0.50 .

5 | RESULTS

5.1 | Single-cylinder settling simulations

Impressions of a single cylinder settling through a fluidized suspension of monodisperse spheres are given in Figure 1. The panels are instantaneous realizations displaying all particles (spheres and cylinder) taking part in the simulation. We show examples of the two ends of the spectrum in terms of overall solids volume fraction $\langle\phi\rangle$: 5% solids and 54% solids. In the lean suspension also impressions of the velocity field are given in the form of velocity magnitude contours. At $\langle\phi\rangle = 0.05$, the cylinder has been released vertically. A cylinder vertically released in a single phase (liquid only) system at the given Archimedes number of ~ 900 quickly flips to a horizontal orientation.²² This also happens in the $\langle\phi\rangle = 0.05$ suspension as can be seen in the second panel from the left in Figure 1. Different from the single-phase case, the wake behind the cylinder extends over much shorter distance in the 5% suspension with the particles apparently hindering the formation of a long wake, even at this low solids volume fraction.

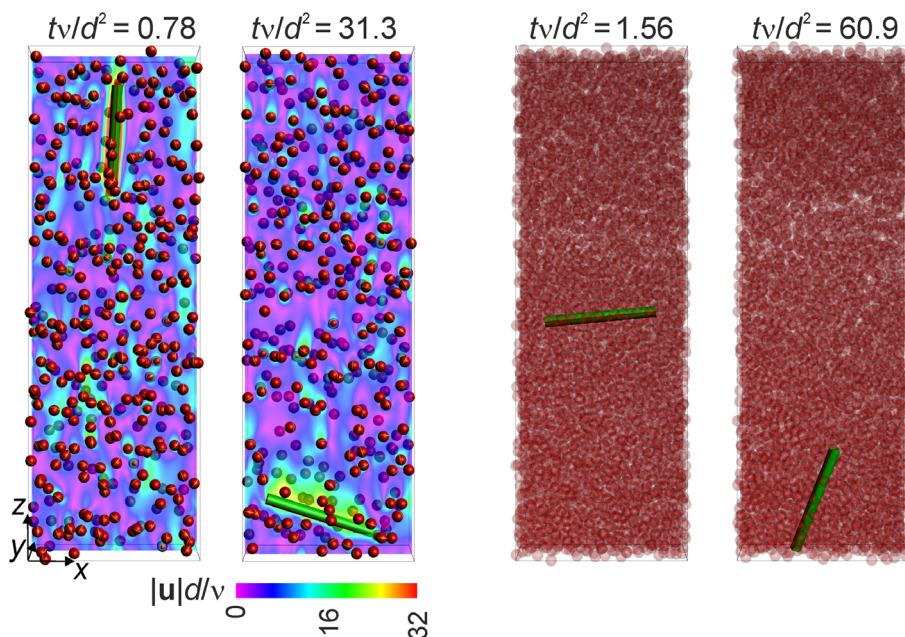


FIGURE 1 A single cylinder (green) settling through liquid with spherical particles (red). Two left panels: $\langle\phi\rangle = 0.05$; two right panels $\langle\phi\rangle = 0.54$. Time after startup as indicated per panel. The left panels show contours of liquid velocity magnitude in the xz -plane that goes through the center of the cylinder. In the right panels the spheres are transparent so as to be able to see the cylinder. For $\langle\phi\rangle = 0.05$ the cylinder was released horizontally; for $\langle\phi\rangle = 0.54$ horizontally. $Ar = 864$. The Cartesian coordinate system is defined in the left panel.

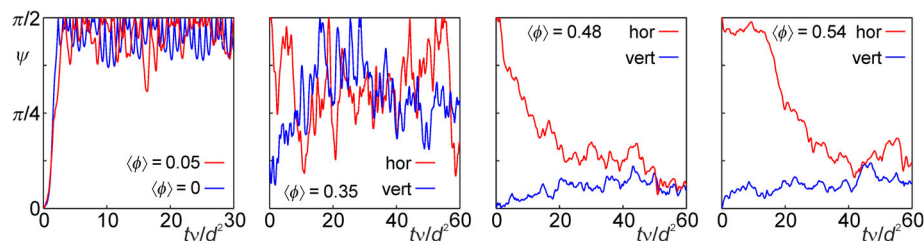


FIGURE 2 Sample time series of the orientation angle ψ of a single cylinder settling through liquid with spherical particles at $Ar = 864$. From left to right: 1st: comparison between a cylinder settling through clear liquid and through a suspension with $\langle\phi\rangle = 0.05$; 2nd: $\langle\phi\rangle = 0.35$ with the cylinder either released vertically or horizontally (as indicated); 3rd: $\langle\phi\rangle = 0.48$ with the cylinder either released vertically or horizontally; 4th: $\langle\phi\rangle = 0.54$ with the cylinder either released vertically or horizontally.

An opposite orientation change of the cylinder occurs in the dense suspension, see Figure 1 (the right two panels). After releasing the cylinder horizontally in the $\langle\phi\rangle = 0.54$ suspension it rotates to a more or less stable vertical orientation. The same cylinder released vertically in the same suspension stays close to its original orientation while settling, as shown in Figure 2 (most right panel). Figure 2 shows time series of the angle ψ between the center line of the cylinder and the vertical direction. In addition to the observations described above related to Figure 1, it shows a strongly fluctuating orientation angle ψ for $\langle\phi\rangle = 0.35$, and the flipping from vertical to horizontal in a no-spheres case and in a $\langle\phi\rangle = 0.05$ case. Without spheres, the cylinder wobbles periodically; adding 5% spheres clearly disturbs this wobbling periodicity. We thus observe—at a fixed value of $Ar = 864$ —that at low $\langle\phi\rangle$ the stable orientation for settling is horizontal and at high $\langle\phi\rangle$ it is vertical. At an intermediate value of $\langle\phi\rangle = 0.35$ the cylinder's orientation strongly fluctuates.

The transition from horizontal settling for lean (low $\langle\phi\rangle$) suspensions to vertical settling in dense suspensions has been investigated further by a range of simulations with cylinders released vertically and horizontally in suspensions with varying solids volume fraction. Most

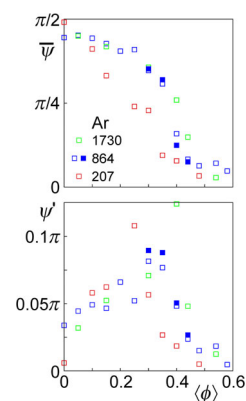


FIGURE 3 Time-averaged orientation angle $\bar{\psi}$ and the root-mean square value of the fluctuations of the angle ψ' as a function of overall solids volume fraction $\langle\phi\rangle$ for three values of Ar as indicated. Cylinders were released vertically except for the cases having a filled blue square that have horizontal release.

of these simulations are at $Ar = 864$; however, also $Ar = 207$ and 1730 have been considered. The results are in Figure 3. It shows the time-average orientation angle $\bar{\psi}$ and its root-mean-square value ψ'

with averages taken over a dynamically steady portion of the orientation time series between t_1 and $t_2 > t_1$ such that $(t_2 - t_1)\nu/d^2 \geq 20$. If we first focus on the results for $Ar = 864$ (the blue symbols) one sees

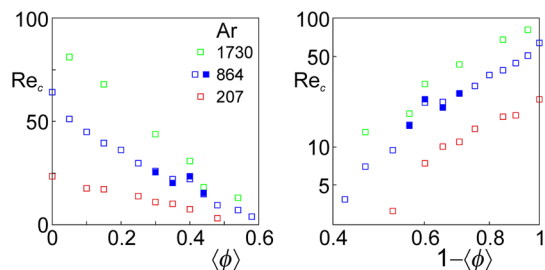


FIGURE 4 Cylinder Reynolds number Re_c as a function of overall solids volume fraction $\langle\phi\rangle$ for three values of Ar as indicated. Cylinders were released vertically except for the cases having a filled blue square. Left and right are two representations of the same data. Left $\langle\phi\rangle$ versus Re_c on linear scales; right $1 - \langle\phi\rangle$ versus Re_c on logarithmic scales.

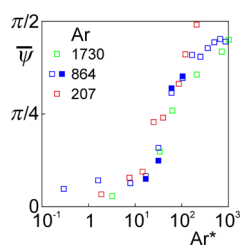


FIGURE 5 Time-averaged orientation angle $\bar{\psi}$ as a function of the modified Archimedes number Ar^* (defined in the text). Same data and same legend as in the top panel of Figure 3.

preferential horizontal settling if $\langle\phi\rangle \leq 0.25$; mostly vertical settling if $\langle\phi\rangle > 0.40$ and a transition range in between these two values. The transition range is associated with high levels of ψ' , that is, in the transition range the orientation angle of the cylinder fluctuates strongly while it moves through the suspension of spheres. This was already noted in the time series of Figure 2—the panel with $\langle\phi\rangle = 0.35$. The results for vertically and horizontally released cylinders (open and closed blue symbols respectively in Figure 3) agree fairly well in terms of $\bar{\psi}$ as well as ψ' with the largest differences in the transition zone likely being the result of statistical uncertainty. As expected, the initial orientation has no influence on the long-time orientational behavior of the cylinder. At the high end of $\langle\phi\rangle$, angle fluctuations approach zero. The cylinder moves vertically with only weak excursions from its orientation. At low $\langle\phi\rangle$ the fluctuations are mostly due to wobbling (see Figure 2, left panel) with only a slight increase in ψ' as $\langle\phi\rangle$ goes from ≈ 0 (no spheres) to 0.05. Only when we enter the transition (at $\langle\phi\rangle \approx 0.30$), ψ' increases significantly.

Similar observations apply to $Ar = 207$ (red symbols in Figure 3) and $Ar = 1730$ (green symbols) with, however, a shift over the x -axis as compared with $Ar = 864$. For $Ar = 207$ the horizontal-to-vertical transition zone shifts to lower values of $\langle\phi\rangle$ which means that it is more likely for the cylinder to settle vertically if the Archimedes number decreases. An increase in Ar is mostly felt at the high end of $\langle\phi\rangle$. At $Ar = 1730$ and $\langle\phi\rangle = 0.44$ we are clearly in the transition range where this was not so for $Ar = 864$. At the lower $\langle\phi\rangle$ end, the $Ar = 1730$ results closely follow those with $Ar = 864$.

In Figure 4 it is shown how the Reynolds number associated with the cylinder depends on the solids volume fraction $\langle\phi\rangle$ and on Ar . This Reynolds number is defined as $Re_c = u_{\text{slip,vc}} d_e / \nu$ with $u_{\text{slip,vc}} \equiv$

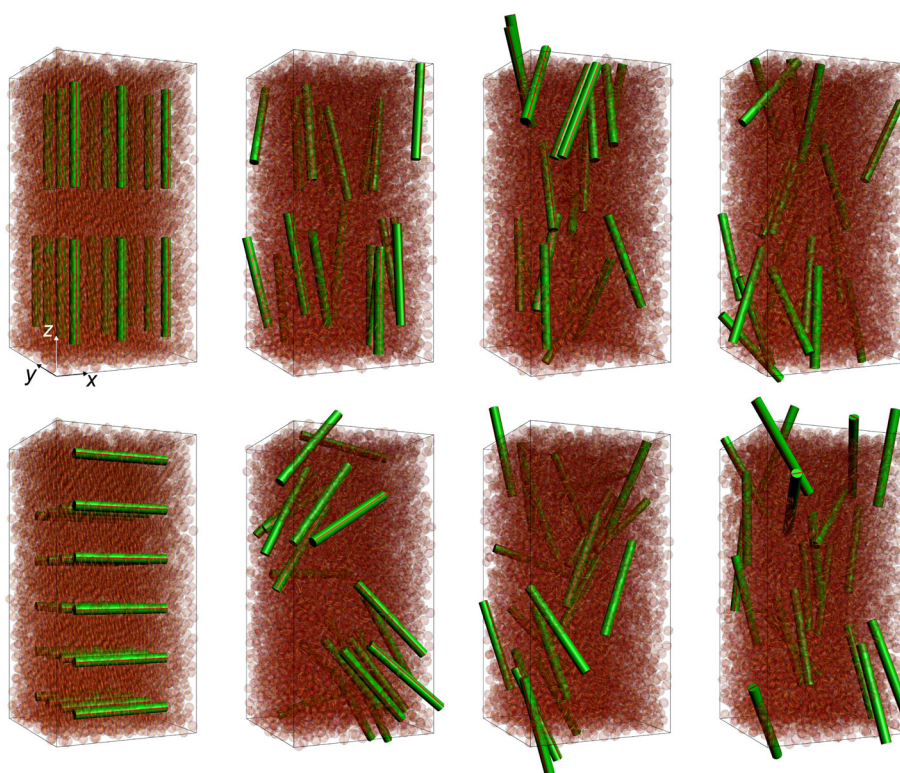


FIGURE 6 Evolution of co-fluidized systems with $\langle\phi\rangle = 0.48$, $\langle\phi_c\rangle/\langle\phi\rangle = 0.05$, and $Ar = 864$; starting with vertical cylinders (top) and horizontal cylinders (bottom). From left to right instantaneous realizations at moments $t\nu/d^2 = 0, 6.25, 12.5, \text{ and } 25$, respectively. The spheres have been made semi-transparent for better visibility of the cylinders.

$\overline{u_z} - \overline{u_{cz}}$ the average vertical slip velocity of the cylinder, $\overline{u_z}$ the volume and time-averaged vertical superficial velocity, $\overline{u_{cz}}$ the time-averaged vertical cylinder velocity, and $d_e = d\sqrt{\frac{3}{2}}\ell/d$ the cylinder's equivalent diameter. The velocity $u_{\text{slip,vc}}$ in this Reynolds definition is the average vertical velocity of the cylinder one would observe in an experiment while it settles through a fluidized spheres suspension.

The two panels in Figure 4 represent the same data in two different ways. In the left panel we see—as expected—a decrease of Re_c with increasing $\langle\phi\rangle$ (hindered settling²³), and an increase with Ar . There is some evidence of the transition between vertical and horizontal settling. In the interval $0.35 \leq \langle\phi\rangle \leq 0.40$ there is a hiccup—for $Ar = 864$ —in the decrease of Re_c with increasing $\langle\phi\rangle$ which likely is the result of the settling orientation transition from horizontal to vertical. In the right panel of Figure 4 this transition can be witnessed more clearly. Here the data are presented in a “Richardson-Zaki” way.²³ Given that, according to Richardson and Zaki, hindered settling speed is proportional to $(1 - \langle\phi\rangle)^N$ we plot Re_c versus $(1 - \langle\phi\rangle)$ in a double logarithmic way. We see that the orientation transition is correlated to a slight but significant change of slope, the latter representing the exponent N .

The effect of the Archimedes number on the orientation of a settling slender cylinder through a single phase Newtonian and non-Newtonian fluids has been studied extensively by experimental as well as computational means.^{22,24} When the cylinder is released vertically in a Newtonian fluid it has been demonstrated that it will eventually turn horizontally²⁴ where the time this takes depends on the Archimedes number; the higher Ar , the shorter this time. Above we have observed fundamentally different behavior for a cylinder settling through a suspension of spheres with—for high solids volume fractions—a stable vertical orientation.

As a way to further interpret the behavior of the cylinder—specifically its orientation—as it settles through the spheres suspension we view the spheres suspension as a continuum fluid with an effective viscosity and density. This is a somewhat crude approach given that the diameter of the cylinder is the same as the diameter of the spheres so that the cylinder does not really experience the spheres suspension as a continuum but rather encounters the spheres as individual particles. For the effective density of the suspension we take the mixture density $\rho_m = \langle\phi\rangle\rho_p + (1 - \langle\phi\rangle)\rho$; for the effective viscosity the Krieger-Dougherty²⁵ expression $\nu_{\text{eff}}\rho_m = \nu\rho(1 - \langle\phi\rangle/\phi_{\text{mx}})^{-2.5\phi_{\text{mx}}}$ where we have set the random-close-packing solids volume fraction to $\phi_{\text{mx}} = 0.64$. This then enables the definition of a modified Archimedes number $Ar^* = (\gamma_{\text{eff}} - 1)gd^3/\nu_{\text{eff}}^2$ with $\gamma_{\text{eff}} = \rho_p/\rho_m$.

In Figure 5 the data for the average angle $\overline{\psi}$ as plotted in Figure 3 (top panel) have been replotted as $\overline{\psi}$ as a function of Ar^* . To capture the wide range of Ar^* it is plotted on a logarithmic scale. Despite the significant scatter in Figure 5, the overall trend is clear: a transition from vertical settling at low Ar^* to horizontal settling at high Ar^* where the solids volume effect as observed in Figure 3 has now been captured through the way effective viscosity and density depend on $\langle\phi\rangle$. Note that an increase of $\langle\phi\rangle$ makes Ar^* smaller for two reasons: its effect on the density ratio *and* on the effective viscosity.

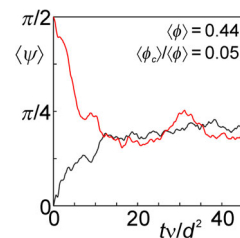


FIGURE 7 Time series of the volume-average cylinder orientation angle $\langle\psi\rangle$ in co-fluidization simulations. Comparison between vertically and horizontally released cylinders. $Ar = 864$.

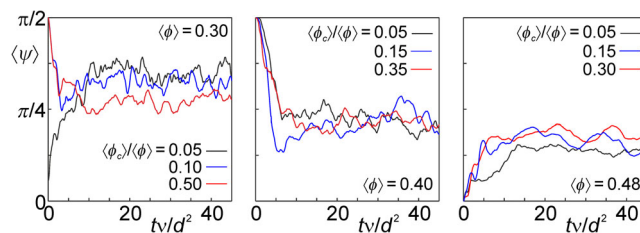


FIGURE 8 Time series of the average cylinder orientation angle $\langle\psi\rangle$ in co-fluidization simulations. From left to right: $\langle\phi\rangle = 0.30, 0.40, \text{ and } 0.48$, respectively. Relative solids volume of cylinders $\langle\phi_c\rangle/\langle\phi\rangle$ as indicated. In all cases $Ar = 864$.

On a more tentative level, the concept of the spheres suspension as a continuum through which the cylinder settles might provide hints for the understanding of vertical settling under dense conditions in terms of viscoelastic effects. It has been argued that if only viscous and inertial forces are at play, a cylinder eventually turns horizontal when settling.²⁴ Experiments show that in liquids exhibiting elasticity, under certain conditions (mostly related to visco-elastic time scales) a vertical orientation of the cylinder is the stable one.²⁴ Given that dense, non-Brownian hard-sphere suspensions exhibit viscoelastic behavior^{26,27} this might be relevant for our observations of vertical settling under certain circumstances. It would require further study to (quantitatively) substantiate this.

5.2 | Co-fluidization of cylinders and spheres

In this section on co-fluidization of multiple cylinders and spheres, only the base-case Archimedes number, $Ar = 864$, has been considered. Figure 6 shows impressions of how simulations are started and how they evolve with an emphasis on the cylinders, their position and orientation. In a random spheres-only assembly, space for the cylinders is created by removing spheres that overlap with the cylinders. Once the cylinders are placed the simulation is started from rest. Our main interest is in the statistical properties of cylinder and sphere motion after a dynamic steady state has been reached. To assess when this is, we keep track of the volume-average orientation angle $\langle\psi\rangle$ as a function of time. By comparing vertically and horizontally released cylinders (see Figures 7 and 8) it becomes clear that after

some time—approximately 15 viscous time scales (corresponding to a convective time of $u_{\text{slip,vc}}t/d \approx 75$)—the system has forgotten its initial condition and has entered a dynamic steady state.

We expect to observe similar preferential cylinder orientations in fluidization with a relatively small number of cylinders as we saw when a single cylinder settles through a suspension of spheres as discussed previously. This is confirmed in Figure 8 that shows time series of $\langle \psi \rangle$ for $\langle \phi \rangle = 0.30, 0.40, \text{ and } 0.48$. For the lowest relative amount of cylinder volume considered in this study— $\langle \phi_c \rangle / \langle \phi \rangle = 0.05$ —the time-averaged orientation angle in steady state ($\overline{\langle \psi \rangle}$, the volume and time-averaged orientation angle) decreases with increasing $\langle \phi \rangle$: $\overline{\langle \psi \rangle} \approx 0.35\pi, 0.20\pi, \text{ and } 0.13\pi$ for $\langle \phi \rangle = 0.30, 0.40, \text{ and } 0.48$, respectively. These angles are similar to or slightly higher than single-cylinder

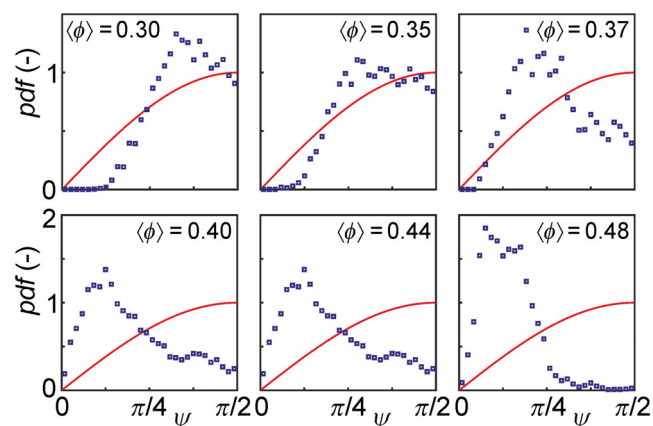


FIGURE 9 Probability density functions (pdf's) of the orientation angle ψ in co-fluidization simulations over a range of overall solids volume fractions. All cases have $\langle \phi_c \rangle / \langle \phi \rangle = 0.05$ and $Ar = 864$. The red curve is $\sin \psi$ which is what an isotropic orientation distribution would look like.

angles at the corresponding solids volume fractions, see Figure 3 (top panel, data for $Ar = 864$). Adding more cylinder volume (and taking out the same amount of sphere volume), that is, increasing $\langle \phi_c \rangle / \langle \phi \rangle$, makes $\overline{\langle \psi \rangle}$ smaller for $\langle \phi \rangle = 0.30$ and larger for $\langle \phi \rangle = 0.48$; for $\langle \phi \rangle = 0.40$ there is no clearly discernable trend with $\langle \phi_c \rangle / \langle \phi \rangle$ (see Figure 8).

More detailed information on how the cylinders orient under a range of conditions is in Figures 9 and 10 that show ψ distributions. As a reference, each panel of these figures includes $\sin \psi$ which is the way ψ would be distributed for an isotropically oriented random assembly of cylinders. Figure 9 focuses on $\langle \phi_c \rangle / \langle \phi \rangle = 0.05$, while Figure 10 investigates trends with increasing $\langle \phi_c \rangle / \langle \phi \rangle$. Some data in Figure 9 have been duplicated in Figure 10.

It is remarkable to see in Figure 9 that for $\langle \phi \rangle \leq 0.37$ the cylinders completely avoid going vertical, while for $\langle \phi \rangle = 0.48$ virtually no horizontally oriented cylinder is encountered. For $\langle \phi \rangle \geq 0.40$ the angle distribution peaks at $\psi \approx 0.1\pi$.

Increasing $\langle \phi_c \rangle / \langle \phi \rangle$ from 0.05 to higher values makes the angle distributions generally less extreme. This is shown in Figure 10. At $\langle \phi \rangle = 0.30$ the zero plateau of the pdf near $\psi = 0$ has vanished when $\langle \phi_c \rangle / \langle \phi \rangle \geq 0.15$ and the angle distribution gets closer to an isotropic distribution with, however, a consistent underrepresentation of horizontal cylinders. For $\langle \phi \rangle = 0.48$ the zero plateau near horizontal orientation ($\psi = \pi/2$) only shows for $\langle \phi_c \rangle / \langle \phi \rangle = 0.05$ and has disappeared when $\langle \phi_c \rangle / \langle \phi \rangle = 0.15$. All angle distributions for $\langle \phi \rangle = 0.48$ and 0.44 show a pronounced preference for near-vertical cylinder orientation. From experiments, this is a phenomenon known to also occur in dense cylinder-only settling through liquid or in fluidization by liquid.^{28,29}

From Figure 10 it is clear that the relative amount of cylinder volume impacts the co-fluidization behavior of the system at large and the behavior of the cylinders in particular. To investigate to what extent this is the result of enhanced direct cylinder-cylinder interaction upon an increase of $\langle \phi_c \rangle / \langle \phi \rangle$, the average coordination number

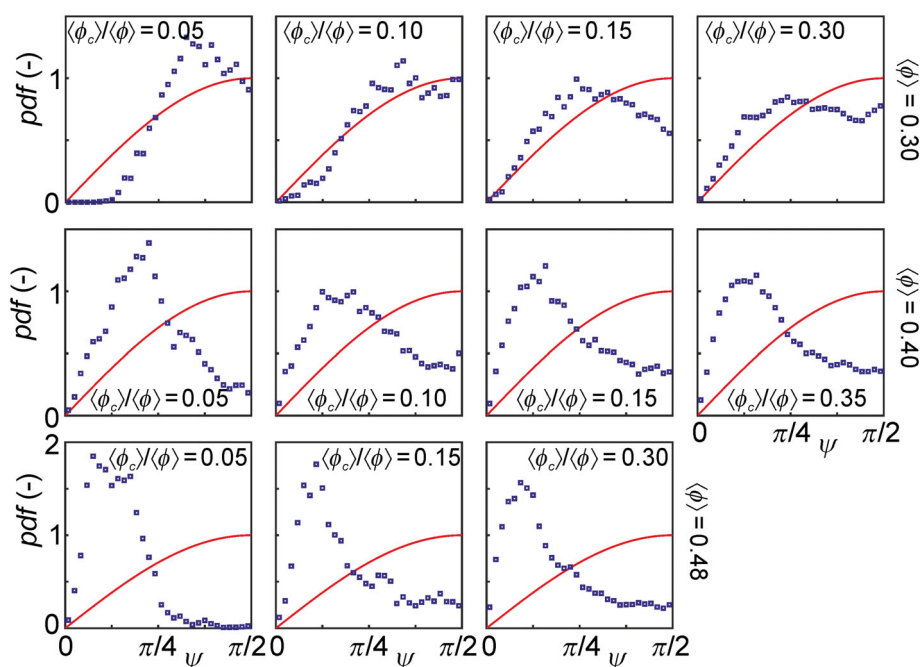


FIGURE 10 Probability density functions (pdf's) of the orientation angle ψ in co-fluidization simulations. From left to right the relative amount of cylinder volume $\langle \phi_c \rangle / \langle \phi \rangle$ increases. From top to bottom $\langle \phi \rangle$ increases. $Ar = 864$. The red curve is $\sin \psi$.

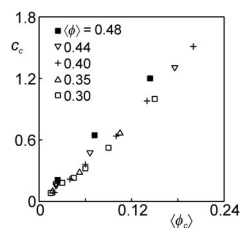


FIGURE 11 Average coordination number of cylinder-cylinder contacts c_c as a function of the cylinder volume fraction $\langle\phi_c\rangle$ for a range of overall solids volume fractions $\langle\phi\rangle$ as indicated.

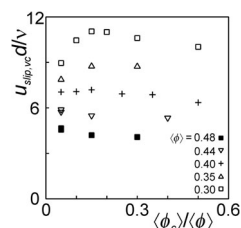


FIGURE 13 Average vertical cylinder slip velocity $u_{\text{slip},vc}$ as a function of the relative amount of cylinder volume $\langle\phi_c\rangle/\langle\phi\rangle$ for a range of overall solids volume fractions $\langle\phi\rangle$.

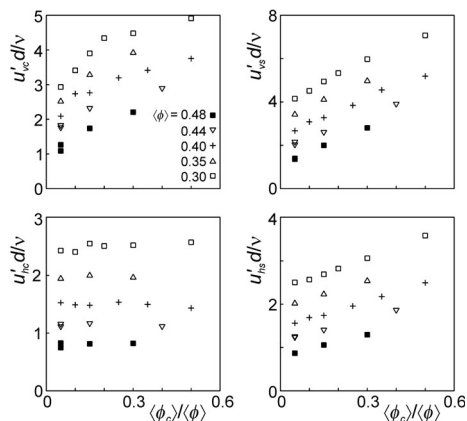


FIGURE 12 Root-mean-square values of fluctuating particle velocities (non-dimensionalized with ν/d) as a function of the relative amount of cylinder volume $\langle\phi_c\rangle/\langle\phi\rangle$ for a range of overall solids volume fractions $\langle\phi\rangle$. Left panels: cylinder velocities in vertical and horizontal direction (u'_{vc} and u'_{hc} , respectively). Right panels: sphere velocities in vertical and horizontal direction (u'_{vs} and u'_{hs} , respectively).

of cylinder-cylinder contact was determined. For a large number of realizations of each simulation the number of contacts between cylinders was counted. The average coordination number c_c then is the average number of cylinders a cylinder is in contact with at any moment in time. Obviously, c_c increases if the cylinder volume fraction $\langle\phi_c\rangle$ increases, see Figure 11. It does so, however, in an approximately linear manner and largely independent of the overall solids volume fraction $\langle\phi\rangle$, that is, independent of the number of spheres present. The coordination number c_c almost uniquely depends on $\langle\phi_c\rangle$; most data points in the figure follow the same trend line, only the $\langle\phi\rangle = 0.48$ data tend to slightly higher c_c values. We interpret this as evidence that the cylinders are distributed over the flow volume in a way that is independent of $\langle\phi\rangle$. In other words, the cylinders show no tendency to cluster or preferentially concentrate. This then indicates that the different ways in which the orientation angle distributions change with increasing $\langle\phi_c\rangle/\langle\phi\rangle$ for different $\langle\phi\rangle$ —as shown in Figure 10—are not the result of cylinders clustering.

We note that the ψ distributions are getting less extreme upon increasing $\langle\phi_c\rangle/\langle\phi\rangle$. This could mean that the increased number of cylinders stir the fluidized system more vigorously (as also observed in Ref. [10]) thus deviating the cylinders more from their inherent

preferential orientations (horizontal for lower $\langle\phi\rangle$, vertical for higher $\langle\phi\rangle$). To test this hypothesis, we have determined spheres and cylinders velocity fluctuation levels; see Figure 12 that shows root-mean-square (rms) velocity values. It distinguishes between spheres and cylinders and horizontal and vertical velocity components. As has been observed previously in liquid fluidization/sedimentation, the vertical fluctuation levels are approximately larger by a factor of 2 than the ones in horizontal direction.²⁹ An increasing trend with $\langle\phi_c\rangle/\langle\phi\rangle$ is observed for the horizontal and vertical sphere rms values as well as for the vertical cylinder velocity fluctuations. The horizontal component of the cylinder velocity fluctuations is not sensitive to $\langle\phi_c\rangle/\langle\phi\rangle$. We conclude that the fluidized system gets more agitated when the amount of cylinder volume is increased. This then contributes to a widening of the orientation angle distribution upon increasing the relative number of cylinders. However, also the increased direct contact between cylinders (see Figure 11) will have its influence on the angle distribution.

It is not obvious how to distinguish between cause and effect when it comes to relating cylinder orientation angle distributions and cylinder velocity fluctuations. For the cylinders, a wider angle distribution contributes to more vertical velocity fluctuations since orientation angle and vertical velocity are related. A horizontal cylinder will experience more drag than a vertical one and will move slower through the spheres suspension. Figure 13 shows this effect in terms of average vertical cylinder slip velocities. With increasing $\langle\phi_c\rangle/\langle\phi\rangle$ at $\langle\phi\rangle = 0.30$ and 0.35 , cylinders get less horizontal (see Figure 10 for $\langle\phi\rangle = 0.30$) and—as a result—increase their slip velocity. The opposite happens for $\langle\phi\rangle = 0.48$ and 0.44 where slip velocities get smaller because cylinders get less vertical with larger $\langle\phi_c\rangle/\langle\phi\rangle$.

6 | CONCLUSIONS

This article reports on particle-resolved simulations of the behavior of tall rigid cylinders in a suspension of spherical particles in a Newtonian liquid over a range of conditions. The main dependencies investigated are those with the overall solids volume fraction as well as those with the relative amount of solids volume of the cylinders. We have restricted the simulations to a single cylinder aspect ratio ($\ell/d = 10$) and a single solid over fluid density ratio ($\rho_p/\rho = 2.0$). The Archimedes numbers are such that overall we have been dealing with laminar flow

with Reynolds numbers associated to particle slip velocities and velocity fluctuation levels of order 10.

The eventual orientation of a single cylinder settling through a spheres suspension depends strongly on the solids volume fraction of the latter. At low solids volume fraction the cylinder eventually assumes—on average—a horizontal orientation. At high solids volume fraction $\langle\phi\rangle$ it eventually settles vertically. The transition range depends on the Archimedes number. For the mostly investigated value of $Ar = 864$, the transition range roughly is $0.3 \leq \langle\phi\rangle \leq 0.4$. In this range, the angle between the cylinder's centerline and the vertical fluctuates strongly. The change in average orientation with $\langle\phi\rangle$ was noticeable in the average slip velocity of the cylinder as a change in slope in the logarithmic hindered settling plot displaying $1 - \langle\phi\rangle$ versus the Reynolds number based on the cylinder slip velocity.

The trend of preferential orientation persists when more cylinders are added to the system. With a relative amount of cylinder volume of $\langle\phi_c\rangle/\langle\phi\rangle = 0.05$, co-fluidized cylinders in dense systems almost completely avoid getting horizontal. Conversely, no vertical cylinders are encountered for the relatively low solids volume fraction of $\langle\phi\rangle = 0.30$. Increasing the relative amount of cylinder volume makes the orientation angle distributions less extreme. At the same time it was noted that velocity fluctuation levels of the spheres increase with more cylinders in the system; more cylinders stir the fluid bed more vigorously. The cylinders' fluctuating velocity levels in vertical direction are also increasing with $\langle\phi_c\rangle/\langle\phi\rangle$ while the horizontal velocity fluctuations are insensitive to $\langle\phi_c\rangle/\langle\phi\rangle$. Finally, as for the single cylinders, the average vertical cylinder slip velocities to some extent reflect the changes in average orientation of the cylinders, that is, a change to more vertical orientation increases slip velocity and vice versa.

It is important to realize that the work described in this article is purely computational and is in need of experimental validation. There are ample avenues for interesting experimental work. If it would be possible to create refractive index matched liquid-spheres systems³⁰ one could visualize the cylinder behavior quantitatively and test hypotheses with regards to orientation angle (distributions) of single and multiple cylinders as a function of the parameters that were varied in this article. Given the modest Reynolds numbers, these could be relatively small-scale (order 0.1 m) experimental systems with order mm diameter particles. From a computational perspective there is room for enhancing the spatial resolution of the simulations to try and further verify the results. Future work will involve the effect of cylinder flexibility³¹ on the way they orient and organize themselves when co-fluidized with spheres.

Another—more theoretical—avenue for future research is aimed at obtaining a better understanding of preferential vertical orientation of single cylinders moving through dense spheres suspensions and exploring the potential role of elastic properties of the suspension in this respect.

AUTHOR CONTRIBUTIONS

Jos Derksen: Conceptualization (lead); data curation (lead); formal analysis (lead); investigation (lead); methodology (lead); resources

(lead); software (lead); validation (lead); visualization (lead); writing – original draft (lead); writing – review and editing (lead).

DATA AVAILABILITY STATEMENT

Data available on request from the authors.

ORCID

Jos J. Derksen  <https://orcid.org/0000-0002-9813-356X>

REFERENCES

1. Wylie JJ, Koch DL, Ladd AJC. Rheology of suspensions with high particle inertia and moderate fluid inertia. *J Fluid Mech.* 2003;480:95-118.
2. Van der Hoef MA, Beetstra R, Kuipers JAM. Lattice-Boltzmann simulations of low-Reynolds-number flow past mono- and bidisperse arrays of spheres: results for the permeability and drag force. *J Fluid Mech.* 2005;528:233-254.
3. Tavanashad V, Passalacqua A, Subramaniam S. Particle-resolved simulation of freely evolving particle suspensions: flow physics and modeling. *Int J Multiphase Flow.* 2021;135:103533.
4. Derksen JJ, Sundaresan S. Direct numerical simulations of dense suspensions: wave instabilities in liquid-fluidized beds. *J Fluid Mech.* 2007;587:303-336.
5. Lu L, Yu J, Gao X, Xu Y, Shahnam M, Rogers WA. Experimental and numerical investigation of sands and Geldart A biomass co-fluidization. *AIChE J.* 2020;66:e16969.
6. Chen X, Zhong W, Heindel TJ. Using stereo XPTV to determine cylindrical particle distribution and velocity in a binary fluidized bed. *AIChE J.* 2019;65:520-535.
7. Fotovat F, Ansari R, Hemati M, Simonin O, Chaouki J. Sand-assisted fluidization of large cylindrical and spherical biomass particles: experiments and simulation. *Chem Eng Sci.* 2015;126:543-559.
8. Lu X, Bertei A, Finegan DP, et al. 3D microstructure design of lithium-ion battery electrodes assisted by X-ray nano-computed tomography and modelling. *Nat Commun.* 2020;11:2079.
9. Kwade A, Haselrieder W, Leithoff R, Modlinger A, Dietrich F, Droeder K. Current status and challenges for automotive battery production technologies. *Nat Energy.* 2018;3:290-300.
10. Derksen JJ. Liquid co-fluidization of cylinders and spheres. *Can J Chem Eng.* 2022;100:2623-2631.
11. Succi S. *The Lattice Boltzmann Equation for Fluid Dynamics and beyond.* Oxford University Press; 2001.
12. Peskin CS. Flow patterns around heart valves—numerical methods. *J Comput Phys.* 1972;10:252-271.
13. Somers JA. Direct simulation of fluid flow with cellular automata and the lattice-Boltzmann equation. *Appl Sci Res.* 1993;51:127-133.
14. Eggels JGM, Somers JA. Numerical simulation of free convective flow using the lattice-Boltzmann scheme. *Int J Heat Fluid Flow.* 1995;16:357-364.
15. Ten Cate A, Nieuwstad CH, Derksen JJ, Van den Akker HEA. PIV experiments and lattice-Boltzmann simulations on a single sphere settling under gravity. *Phys Fluids.* 2002;14:4012-4025.
16. Kodam M, Bharadwaj R, Curtis J, Hancock B, Wassgren C. Cylindrical object contact detection for use in discrete element method simulations. Part I—contact detection algorithms. *Chem Eng Sci.* 2010;65:5852-5862.
17. Derksen JJ. Liquid fluidization with cylindrical particles: highly resolved simulations. *AIChE J.* 2019;65:e16594.
18. Nguyen N-Q, Ladd AJC. Lubrication corrections for lattice-Boltzmann simulations of particle suspensions. *Phys Rev E.* 2002;66:046708.
19. Kim S, Karrila SJ. *Microhydrodynamics: Principles and Selected Applications.* Butterworth-Heinemann; 1991.

20. Feng ZG, Michaelides E. Robust treatment of no-slip boundary condition and velocity updating for the lattice-Boltzmann simulation of particulate flows. *Comput Fluids*. 2009;38:370-381.
21. Kuipers JB. *Quaternions and Rotation Sequences*. Princeton University Press; 1999.
22. Jinghan X, Zhang L, Lu M, Lu J, Derksen JJ. Experiments and simulations of settling cylinders over a wide range of Archimedes numbers. *Can J Chem Eng*. 2022;1.
23. Richardson JF, Zaki WN. Sedimentation and fluidisation. Part 1. *Trans Inst Chem Eng*. 1954;32:35-53.
24. Liu YJ, Joseph DD. Sedimentation of particles in polymer solutions. *J Fluid Mech*. 1993;255:565-595.
25. Krieger IM, Dougherty TJ. (1959) a mechanism for non-Newtonian flow in suspensions of rigid spheres. *Trans Soc Rheol*. 1959;3: 137-152.
26. Van der Werff JC, De Kruif CG, Blom C, Mellema J. Linear viscoelastic behavior of dense hard-sphere dispersions. *Phys Rev A*. 1989;39: 795-807.
27. Mason TG, Weitz DA. Linear viscoelasticity of colloidal hard sphere suspensions near the glass transition. *Phys Rev Lett*. 1995;75:2770-2773.
28. Herzhaft B, Guazzelli E. Experimental study of the sedimentation of dilute and semi-dilute suspensions of fibres. *J Fluid Mech*. 1999;384: 133-158.
29. Guazzelli É, Hinch J. Fluctuations and instability in sedimentation. *Annu Rev Fluid Mech*. 2011;43:97-116.
30. Nicolai H, Guazzelli É. Effect of the vessel size on the hydrodynamic diffusion of sedimenting spheres. *Phys Fluids*. 1995;7:3-5.
31. Derksen JJ. Particle-resolved simulations of liquid fluidization of rigid and flexible fibers. *Acta Mech*. 2020;231:5193-5203.

How to cite this article: Derksen JJ. Settling and fluidization of tall cylinders in solid-liquid suspensions. *AIChE J*. 2023; 69(7):e18072. doi:[10.1002/aic.18072](https://doi.org/10.1002/aic.18072)